

Extracellular vesicles derived from endothelial cells in hypoxia contribute to pulmonary artery smooth muscle cell proliferation in-vitro and pulmonary hypertension in mice

Tianji Chen¹ | Miranda R. Sun¹ | Qiyuan Zhou¹ | Alyssa M. Guzman¹ |
Ramaswamy Ramchandran¹ | Jiwang Chen^{2,3} | Balaji Ganesh⁴ | J. Usha Raj¹

¹Department of Pediatrics, University of Illinois at Chicago, Chicago, Illinois, USA

²Cardiovascular Research Center, University of Illinois at Chicago, Chicago, Illinois, USA

³Department of Medicine, Division of Pulmonary, Critical Care, Sleep and Allergy, University of Illinois at Chicago, Chicago, Illinois, USA

⁴Flow Cytometry Core, Research Resources Center, University of Illinois at Chicago, Chicago, Illinois, USA

Correspondence

Tianji Chen and J. Usha Raj, Department of Pediatrics, University of Illinois at Chicago, 840S. Wood St, M/C 856, Chicago, IL 60612, USA.

Email: tianjic@uic.edu and usharaj@uic.edu

Present address

School of Veterinary Medicine University of Wisconsin-Madison, Madison, Wisconsin.

Funding information

American Heart Association, Grant/Award Number: 18CDA34110301; American Lung Association, Grant/Award Number: RG-416135; National Heart, Lung, and Blood Institute, Grant/Award Numbers: 1R56-HL141206-01, R01HL123804; Gilead Sciences; Chicago Biomedical Consortium

Abstract

In the lung, communication between pulmonary vascular endothelial cells (PVEC) and pulmonary artery smooth muscle cells (PASMC) is essential for the maintenance of vascular homeostasis. In pulmonary hypertension (PH), the derangement in their cell-cell communication plays a major role in the pathogenesis of pulmonary vascular remodeling. In this study, we focused on the role of PVEC-derived extracellular vesicles (EV), specifically their microRNA (miRNA, miR-) cargo, in the regulation of PASMC proliferation and vascular remodeling in PH. We found that the amount of pro-proliferative miR-210-3p was increased in PVEC-derived EV in hypoxia (H-EV), which contributes to the H-EV-induced proliferation of PASMC and the development of PH.

KEYWORDS

extracellular vesicles, microRNAs, pulmonary artery smooth muscle cells, pulmonary hypertension, pulmonary vascular endothelial cells

INTRODUCTION

Pulmonary vascular endothelial cells (PVEC) and pulmonary artery smooth muscle cells (PASMC) are two key cell types involved in the pathogenesis of

pulmonary vascular structural remodeling in pulmonary hypertension (PH) in all forms of PH.^{1,2} PVEC often act as the “signal initiator” in the process of vascular remodeling, affecting the function of PASMC via secretion of bioactive agents,^{1,3–7} transfer of signals

Tianji Chen and Miranda R. Sun authors contributed equally to this study.

This is an open access article under the terms of the Creative Commons Attribution-NonCommercial License, which permits use, distribution and reproduction in any medium, provided the original work is properly cited and is not used for commercial purposes.

© 2021 The Authors. *Pulmonary Circulation* published by John Wiley & Sons Ltd on behalf of Pulmonary Vascular Research Institute.

through myoendothelial junctions (MEJ)⁸ and/or by releasing extracellular vesicles (EV),⁹ in both health and disease.

EV are a heterogeneous family of membrane-limited vesicles originating from the endosome or plasma membrane¹⁰ and are classified into three types based primarily on their size and presumed biogenetic pathways: exosomes (30–100 nm),^{11–14} microvesicles (MV) or ectosomes (100–1000 nm),^{12,15–18} and apoptotic bodies (1–5 μ m),^{12,19} and they carry complex cargo including proteins, lipids, and nucleic acids, and so on.^{10,20,21}

In this study, we first showed that EV released from PVEC in culture in hypoxia (H-EV) induced PASM C proliferation and when given to mice in room air intravenously (i.v.), induced pulmonary vascular remodeling and PH. Next, we investigated the role of the microRNA^{22–25} (miRNA, miR-) cargo in H-EV in mediating these effects. Hypoxia significantly increased the amount of a known “pro-proliferative” miRNA, miR-210-3p in PVEC-derived EV, while inhibition of miR-210-3p in H-EV significantly attenuated the ability of H-EV to induce PH in mice in room air in-vivo, suggesting that miR-210-3p in H-EV plays a major role in H-EV-induced PH in mice in room air. Our study provided the first evidence of the role of endothelium-derived EV in PH as well as the underlying mechanisms.

METHODS AND MATERIALS

Cell culture

Mouse and rat PVEC (mPVEC and rPVEC) were purchased from Cell Biologics and maintained in Endothelial Cell Medium containing 5% fetal bovine serum (FBS), endothelial cell growth factors, and antibiotics (Cell Biologics). Mouse and rat PASM C (mPASM C and rPASM C) were isolated from mouse lungs as we described previously²⁶ and were maintained in SmGM-2 medium (Lonza) containing 5% FBS, growth factors, and 1% penicillin-streptomycin. We also isolated mPASM C from mice exposed to 10% O₂ for 3 weeks and from mice exposed to room air for 3 weeks (controls).

Human pulmonary artery endothelial and smooth muscle cells (hPVEC and hPASM C) were purchased from Lonza and were maintained in EBM-2 and SmGM-2 medium containing FBS and growth factors (Lonza), respectively.²⁶

All cells were maintained in a humidified incubator with a constant supply of 5% CO₂ at 37°C.

Isolation of EV

EV were isolated from cultured mPVEC using a multi-step centrifugation method.^{15,17,18,27} Briefly, after obtaining confluent monolayers of mPVEC, the medium was refreshed with a medium free of FBS or vesicles, and mPVEC were then exposed to room air (normoxia, N) or hypoxia (1% O₂, H). Conditioned medium was collected 24 hours (h) later and cell debris precleared by centrifugation at 2000g for 15 min at 4°C. The supernatant was centrifuged at 20,500g for 1 h at 4°C. Pelleted vesicles (mainly MVs) were washed with ice-cold vesicle-free Dulbecco's phosphate-buffered saline (DPBS) and pelleted again by centrifugation at 20,500g for 1 h at 4°C. Finally, the pelleted vesicles were resuspended in vesicle-free DPBS or lysed in QIAzol Lysis Reagent (Qiagen) for RNA isolation using the miRNeasy kit (Qiagen).

Transmission electron microscope (EM)

EV were mounted on 300-mesh copper grids and stained with phosphotungstic acid (PTA). All specimens were examined with a JEM-1220 transmission EM (JEOL USA) at Electron Microscopy Core of the University of Illinois at Chicago (UIC).

Nanoparticle tracking analysis (NTA)

The vesicle size and number were determined using NTA technology with a NanoSight LM10-HS instrument (Malvern Instruments Ltd.) at the Flow Cytometry Core of UIC. EV were resuspended in vesicle-free DPBS and diluted as needed (typically 1:100 to 1:1000 dilution), and then 1 ml samples were injected into the sample chamber using a sterile NORM-JECT[®] syringe (Henke-Sass Wolf). Images of EV were captured and analyzed by Nanosight NTA 3.2 software. The camera level was set to 11–16 and the detection threshold at 2–5 to get the optimum brightness of images, and each sample was run for 30 s per time for three to four times. For samples in each experiment, the setting was kept constant.

Imaging of EV in the pulmonary vessel wall

We labeled EV with PKH26 dye (Sigma-Aldrich) and then injected 5×10^8 EV into mice through the tail vein. 10 min later, mice were sacrificed and lungs were collected for the frozen tissue section. PKH26-labeled EV were imaged using Zeiss LSM 710 Confocal Microscope

(META) (Zeiss) at the Fluorescence Imaging Core of UIC.

Western blot analysis

Isolated EV were lysed in mRIPA buffer (50 mM Tris pH 7.4, 1% NP-40, 0.25% deoxycholate, 150 mmol/L NaCl, and protease inhibitors). 10 μ g (for EV samples) or 30 μ g (for cell samples) of protein lysate was separated by sodium dodecyl sulfate-polyacrylamide gel electrophoresis and transferred to BA85 nitrocellulose membrane (PROTRAN; Whatman). Proteins were detected with SuperSignal West Pico Chemiluminescent Substrate (Thermo Scientific). The following primary antibodies were used: CD144 (Santa Cruz Biotechnology), α -Tubulin, β -actin, α -smooth muscle actin (α -SMA), calponin, myosin heavy chain (MHC) (Sigma-Aldrich), smooth muscle protein 22- α (SM22 α) (Abcam), Myocardin (R&D Systems), proliferating cell nuclear antigen (PCNA) (Proteintech Group), CD31, protein disulfide isomerase (PDI), endoplasmic reticulum (ER) stress protein 72 (ERp72), receptor-binding cancer antigen expressed on SiSo cells (RCAS1), cytochrome c oxidase (COX) IV (Cell Signaling Technology, Danvers, MA). Detailed information about antibodies is in Table S1.

Flow cytometry analysis

For flow cytometry, EV were resuspended in PBS and incubated with Alexa-488 conjugated Annexin V (mouse, Enzo Lifesciences) for 15 min at 4°C in the dark. Non-specific isotype antibodies served as negative controls.

RNA isolation

Total RNA was isolated using a miRNeasy Mini Kit or miRNeasy Micro Kit (Qiagen) and treated with RNase-Free DNase I (Qiagen),²⁶ quantified with Nanodrop 2000 spectrophotometer (Thermo Scientific) and then used for miRNA deep sequencing (LC Sciences) or quantitative real-time reverse transcription-polymerase chain reaction (qRT-PCR) analysis.

miRNA deep sequencing

Six batches of EV from mPVEC exposed to room air or hypoxia (1% O₂, 24 h) (H-EV vs. N-EV) were collected for miRNA deep sequencing (LC Sciences). Briefly, a small RNA library was generated from RNA isolated from N-EV

and H-EV using the Illumina Truseq™ Small RNA Preparation kit (Illumina). The purified cDNA library was used for cluster generation on Illumina's Cluster Station and then sequenced on Illumina GAIIX (Illumina). Raw sequencing reads (40 nts) were obtained using Illumina's Sequencing Control Studio software version 2.8 (SCS v2.8) following real-time sequencing image analysis and base-calling by Illumina's Real-Time Analysis version 1.8.70 (RTA v1.8.70). The extracted sequencing reads were then normalized under a proprietary pipeline script of LC Sciences (ACGT101-miR v4.2) and used for statistical analysis (Research Informatics Core, UIC).

qRT-PCR

For qRT-PCR analysis of miRNA expression, a poly (A) tail was first added to the 3'-end of miRNAs using a Poly (A) Polymerase Tailing Kit (Epicentre Biotechnologies). Poly (A) tailed-miRNAs were then reverse-transcribed using M-MLV Reverse Transcriptase (Invitrogen) with a poly (T) adaptor, which consists of a poly (T) sequence and a sequence complementary to the universal primer used in the following qRT-PCR analysis. For cell or tissue samples, SNORD44, SNORD47, SNORD48, and/or miR-16 were used as internal controls. qRT-PCR was performed using SYBR Green PCR Master Mix (Applied Biosystems) on StepOnePlus or ViiA 7 Real-Time PCR System (Applied Biosystems). Primer sequences are in Table S2.

Bromodeoxyuridine (BrdU) cell proliferation assay

Cell proliferation was measured using a BrdU cell proliferation assay kit (EMD Millipore).²⁶ Briefly, PASMCMC were plated into a 96-well plate at a density of 3000 cells/well and incubated overnight. BrdU label was added to the culture medium the next day and cells were cultured for another 16–18 h. Colorimetric measurements were carried out on a GloMax®-96 Microplate luminometer (Promega). For proliferation assays of PASMCMC with N- or H-EV, 2 \times 10⁶ or 10⁷ EV were added per well and proliferation was measured 24 h later. For proliferation assay of PASMCMC transfected with miRNA oligos, BrdU label was added 24 h after transfection.

miRNA antagonist and mimics

All miRvana™ miRNA inhibitors and mimics for functional studies were purchased from Ambion, Thermo Fisher Scientific. Negative control miRNA inhibitor #1 or

Negative control miRNA mimic #1 was used as the miRNA inhibitor or mimic control, respectively.

Animal studies

All animals were cared for in accordance with the University of Illinois at Chicago Animal Care Policy. Animal experimental protocols were reviewed and approved by the Institutional Animal Care and Use Committee. Six- to eight-week-old male C57BL/6 mice were purchased from Jackson Laboratory. Details of each animal study were described below. For right ventricular systolic pressure (RVSP) measurements, animals were first anesthetized with ketamine (100 mg/kg body weight) and xylazine (5 mg/kg) via intraperitoneal (i.p.) injection. The anesthetics were given once before each procedure and depth of anesthesia was monitored by toe pinching to determine the loss of reflexes. After RVSP measurement, animals were euthanized under anesthesia followed by lung perfusion/exsanguination.

Assessment of PH in animal studies (PH indices)

RSVP, Fulton's index, and lung vascular remodeling were used as indices of severity of PH.

In-vivo RVSP measurements

To measure RVSP, as a surrogate for pulmonary artery pressure, mice were anesthetized with ketamine/xylazine (100 mg/kg and 5 mg/kg body weight, i.p.) and placed on a heating pad to maintain body temperature. A Millar ultraminiature pressure transducer (1.0 Fr; Millar Instruments) was introduced into the right ventricle (RV) via the jugular vein to obtain pressure measurements.

Measurement of ventricular weights to assess right heart hypertrophy

The RV was dissected from the left ventricle and inter-ventricular septum (LV + S), and the ratios of their weights (RV/[LV + S]) (Fulton's index) was measured and calculated as an index of right ventricular hypertrophy.

Lung vascular morphometry

Lungs were inflated at 20 cm H₂O pressure and fixed with 10% buffered formalin via the trachea. Lungs were

also perfused sequentially with PBS and 10% buffered formalin at the same pressure via the RV. Fixed lungs were paraffin-embedded, cut into 5 μ m sections, and stained with hematoxylin and eosin (H&E) at the Research Histology and Tissue Imaging Core of UIC. The stained slides were scanned using Aperio ScanScope (Leica Biosystems). Pulmonary arterioles, typically 50–100 μ m in diameter, adjacent to bronchioles, were measured for wall thickness, represented by the difference between the area of the entire vessel and the area of the lumen divided by the area of the entire vessel.

To determine if mPVEC-derived EV play a role in hypoxia-induced PH in-vivo, mice were injected with 5×10^8 normoxic (N-EV) or hypoxic (H-EV) suspended in 100 μ l sterile and vesicle-free DPBS per injection, once daily (i.v. via tail vein) for three consecutive days, while in room air. Control mice received an equal volume of DPBS. Three weeks after the first injection, mice were sacrificed and PH indices measured.

To study the role of miR-210-3p in H-EV-induced PH in mice, we first generated H-EV from mPVEC in which miR-210-3p level was inhibited (H-EV [anti-miR-210]). Briefly, mPVEC were transfected with miR-210-3p inhibitors (anti-miR-210; Ambion) or Negative control inhibitors (anti-Neg; Ambion) and then exposed to hypoxia (1% O₂) the next day, in a fresh medium free of FBS and vesicles. EV were collected after 24 or 48 h exposure (H-EV [anti-miR-210] or H-EV [anti-Neg]). Then, mice were injected with H-EV (anti-miR-210) or H-EV (anti-Neg) (10^8 EV per daily injection for three consecutive days, via tail vein) while in room air. three weeks later, mice were sacrificed and PH indices measured.

Statistical analysis

All experiments were repeated at least three times independently. For in-vivo experiments, at least five animals were used in each group, except for experiments with H-EV with anti-miR-210 when $n = 3$ (Figure 5). Student's *t* tests were used when comparing two conditions and a one-way analysis of variance (ANOVA) with Bonferroni correction was used for multiple comparisons using GraphPad Prism 5 (GraphPad) and Microsoft Excel (Microsoft) when applicable. Data are presented as mean \pm SEM. For significant differences, $p < 0.05$, 0.01, and 0.001 was set. The power of in-vivo studies was calculated via <https://www.stat.ubc.ca/~rollin/stats/ssize/n2.html>.

RESULTS

Characterization of PVEC-derived EV

EV collected from mPVEC were round and typically 100–200 nm in diameter under the electronic microscope (EM, Figure S1A), suggesting that these particles are mostly MV (100–1000 nm in diameter^{12,16}). Hypoxia (1% O₂, 24 h) did not alter the shape or size of this EV (Figure S1A). We analyzed the size and number of collected EV using NTA and confirmed that their number and size were unchanged in hypoxia (mode size: N- vs. H-EV: 153.3 nm vs. 139.3 nm, mean size: N- vs. H-EV: 237.6 nm vs. 209.6 nm) (Figure S1B). EV expressed specific endothelial cell marker proteins CD31 and CD144 (Figure S1C), confirming their endothelial origin,¹⁰ and they bound Annexin V, a feature of MV (Figure S1D).^{28,29} EV did not express exosome markers heat shock protein 70 kDa (HSP70)^{30,31} or CD63, ER marker proteins PDI or ERP72, Golgi body marker protein RCAS1, or mitochondria marker protein COX IV (Figure S1E). They expressed very low levels of CD81. These results confirm that the EV we collected in this study were mainly MV, and did not contain large amounts of exosomes or cell organelles by contamination from cell debris.

H-EV induce PASMC proliferation in culture and PH in mice in room air

We incubated mPASMC in room air for 24 h with EV collected from mPVEC in room air (N-EV) or hypoxia (1% O₂, H-EV). mPASMC incubated with PBS served as controls. We measured mPASMC proliferation using BrdU proliferation assay and found that neither low or high dose of N-EV affected mPASMC proliferation, but a low dose of H-EV (2 × 10⁶ EV per 3000 cells) induced mPASMC proliferation slightly and a higher dose of H-EV (10⁷ EV per 3000 cells) significantly induced mPASMC proliferation (Figure 1a). We confirmed that the high dose of H-EV induced mPASMC proliferation by measuring PCNA expression by Western blot analysis (Figure 1b). H-EV did not alter the expression of contractile proteins MHC, α -SMA, calponin, smooth muscle protein 22 α (SM22 α), or myocardin in mPASMC (Figure S2). Similarly, we collected N- and H-EV from rat and human PVEC (rPVEC or hPVEC), and incubated rat and human PASMC (rPASMC or hPASMC) in room air with rPVEC and hPVEC-derived EV, respectively. We found that H-EV, and not N-EV, also induced rat and human PASMC proliferation in a dose-dependent

manner (Figure 1c,d), indicating that these results are valid in different species.

Next, we injected N- or H-EV into C57BL/6 mice in room air through the tail vein daily for three consecutive days. Mice injected with PBS served as controls. Three weeks later, we measured PH indices (Figure 2a) and found that H-EV induced a modest but significant increase of RVSP (Figure 2b), RV hypertrophy (Figure 2c), and pulmonary arterial wall remodeling (Figure 2d,e), whereas N-EV did not. To determine if injected EV were reaching the pulmonary vessels, we injected mice with H-EV labeled with PKH26 Red Fluorescent Cell Membrane Labeling through the tail vein and their lungs were collected 10 min later for frozen section. Using confocal microscopy we confirmed that some of the PKH26-labeled EV localized in the pulmonary vessel wall (Figure S3). Taken together, our results suggest that EV released by PVEC in hypoxia can induce PASMC proliferation, vascular remodeling, and PH.

Hypoxia exposure alters the miRNA cargo in PVEC-derived EV and pulmonary vascular cells

As hypoxia did not alter the phenotype (size, number, shape, or surface markers) of mPVEC-derived EV (Figure S1), the functional effect of H-EV is likely due to a change in their cargo. We performed miRNA deep sequencing to compare the miRNA cargo in N- and H-EV. We set the cutoff for fold change of miRNA levels at 1.2 and identified eight miRNAs whose expression was significantly induced by hypoxia exposure (Figure 3a). Using qPCR analysis, we confirmed that the expression of miR-210-3p, 3057-5p, 212-5p, 34-3p, and 106b-3p were induced in H-EV (Figure 3b). We were unable to detect miR-505-3p using our qPCR analysis (data not shown).

Next, we investigated if hypoxia altered the expression of the above-identified miRNAs in mPVEC, mPASMC, and mouse lungs by qPCR analysis. We found that hypoxia exposure (1% O₂) significantly induced miR-210-3p and 212-5p levels in mPVEC in culture after both 6 h and 24 h and miR-3057-5p levels after 24 h (Figure S4A). In mPASMC, hypoxia exposure only induced the expression of miR-210-3p, while the expression of miR-106b-3p was suppressed at 6 h (Figure S4B). Expression of miR-210-3p, as well as that of miR-212-5p, was induced in mPASMC isolated from mice exposed to hypoxia for 3 weeks (Figure S4C). Hypoxia (10% O₂, 3 weeks) also induced the expression of miR-210-3p, 212-5p, and 34c-3p in mouse whole lungs (Figure S4D).

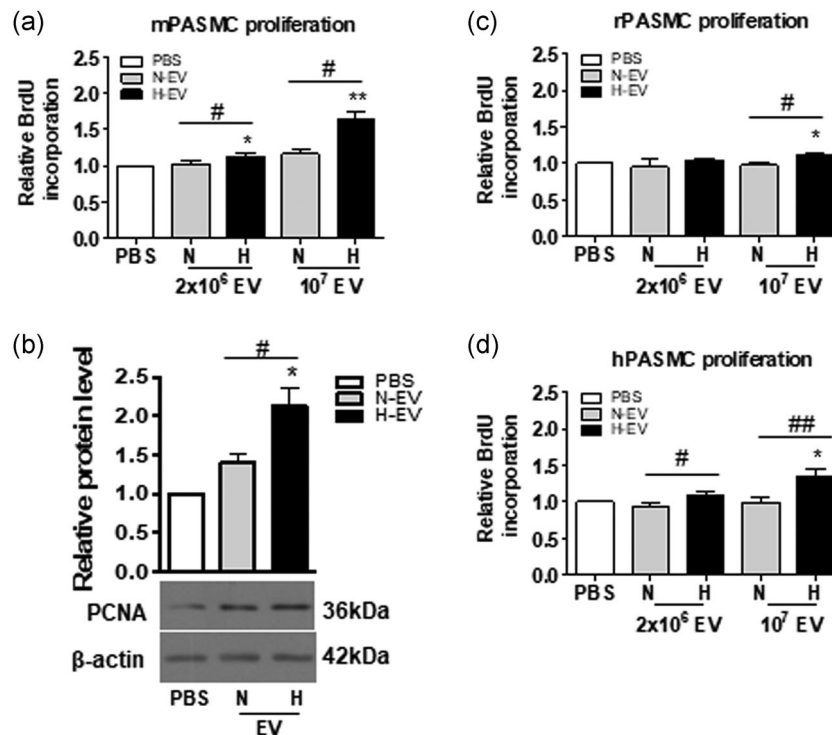


FIGURE 1 Hypoxic PVEC-derived EV (H-EV) induce PASCMM proliferation in culture. (a,b) mPASCMM were incubated in SmGM-2 medium containing PBS, mPVEC-derived N- or H-EV for 24 h in room air. Then mPASCMM proliferation was measured by BrdU proliferation assay (a, $N = 5$) or by measuring PCNA levels using Western blot analysis (b, $N = 4$). Relative BrdU incorporation and PCNA levels were compared to that in mPASCMM incubated with PBS (control, level set as 1). Representative blots and quantification results are shown in b. β -actin was used as loading control. Rat (rPASCMM) (c) and human PASCMM (hPASCMM) (d) in room air were incubated with SmGM-2 medium containing PBS, N- or H-EV derived from rat (rPVEC) and human PVEC (hPVEC), respectively, for 24 h. Then rPASCMM (c) and hPASCMM (d) proliferation were measured by BrdU proliferation assay. Relative BrdU incorporation was compared to that in rPASCMM and hPASCMM incubated with PBS (control, level set as 1). While a low dose of H-EV (2×10^6 EV per 3000 cells) did not alter rPASCMM proliferation significantly, a high dose of H-EV (10^7 EV per 3000 cells) induced rPASCMM proliferation in room air (c). In hPASCMM, while a lower dose of H-EV (2×10^6 EV per 3000 cells) induced hPASCMM proliferation, a higher dose of H-EV (10^7 EV per 3000 cells) induced hPASCMM proliferation further in room air (d). Data are presented as mean \pm SEM. * compared to PBS group; # or ## compared to respective N-EV group; * or #, $p < 0.05$; ##, $p < 0.01$. $N = 3-5$. BrdU, bromodeoxyuridine; EV, extracellular vesicles; hPASCMM, human PASCMM; mPASCMM, mouse PASCMM; mPVEC, mouse PVEC; PASCMM, pulmonary artery smooth muscle cells; PCNA, proliferating cell nuclear antigen; PVEC, pulmonary vascular endothelial cells; rPASCMM, rat PASCMM

MiRNA in PVEC-derived EV regulate PASCMM proliferation

To determine if the above-identified miRNAs contribute to the effect of H-EV on PASCMM proliferation (Figure 1), we transfected mPASCMM with mimics of the identified miRNAs (miR-210-3p, 3057-3p, 212-5p, 34c-3p, and 106b-3p) and then measured mPASCMM proliferation using BrdU proliferation assay. We found that miR-210-3p was the only identified miRNA that induced mPASCMM proliferation (Figure 4), consistent with the findings previously reported by our group and others.^{32,33} All of the remaining miRNAs either inhibited (miR-3057-5p, 212-5p, and 34c-3p) or showed no significant effect (miR-106b-3p) on mPASCMM proliferation (Figure 4). These data suggest that although H-EV contains both

“pro-proliferative” and “antiproliferative” miRNA cargo, the net effect of H-EV is increased proliferation in PASCMM and induction of PH in-vivo, indicating that miR-210-3p may play a predominant role in H-EV-induced PASCMM proliferation and PH in mice. Our speculation can be supported by the finding that miR-210-3p was expressed at a higher level than other identified miRNAs in H-EV and hypoxic PVEC (Figure S5).

MiR-210-3p in H-EV is mainly responsible for H-EV-induced PH and pulmonary vessel remodeling in-vivo

To confirm if miR-210-3p plays a predominant role in H-EV-induced PASCMM proliferation and PH in mice, we

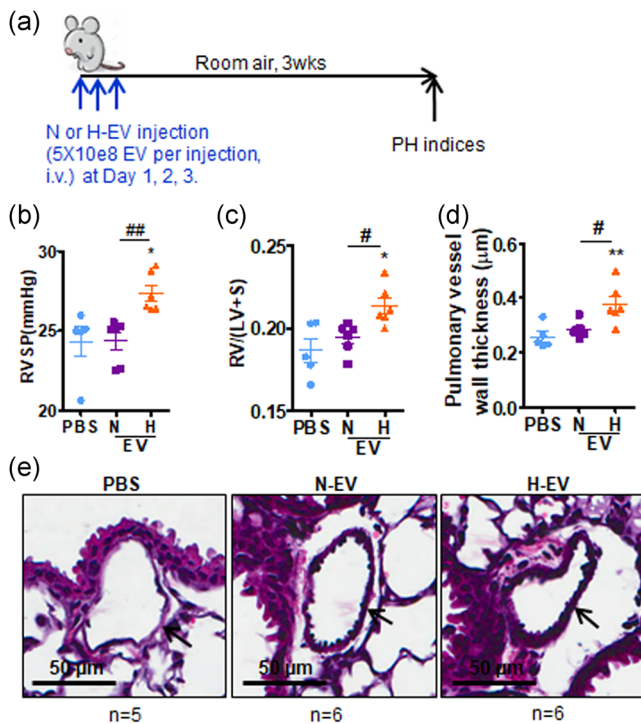


FIGURE 2 Hypoxic PVEC-derived EV (H-EV) induce PH in mice in room air. (a) Experimental design: 6- to 8-week-old C57BL/6 mice were injected intravenously (i.v.) with PBS, mPVEC-derived N- or H-EV (via tail vein) daily for three consecutive days while they were in room air. Three weeks later, RVSP, RV hypertrophy (RV/(LV+S) ratio), and pulmonary vessel wall thickness were measured (b–e) and compared with those in mice injected with PBS. H-EV induced an increase in RVSP (b), RV hypertrophy (c), and pulmonary vessel wall remodeling (d–e) in mice in room air while N-EV did not. Arrows point to vessels. Data are presented as mean \pm SEM. * or ** compared to PBS group; # or ## compared to N-EV group; * or #, $p < 0.05$. ** or ##, $p < 0.01$. (b–e) $N = 5$ for PBS group, $N = 6$ for N- or H-EV groups. EV, extracellular vesicles; H-EV, EV in hypoxia; LV, left ventricle; mPVEC, mouse PVEC; PH, pulmonary hypertension; PVEC, pulmonary vascular endothelial cells; RV, right ventricle; RVSP, right ventricular systolic pressure

generated H-EV containing decreased levels of miR-210-3p (H-EV [anti-miR-210]) by transfecting mPVEC with miR-210-3p inhibitors (anti-miR-210) and then collecting H-EV from these cells. mPVEC transfected with Negative control miRNA inhibitors (anti-Neg) were used to generate control H-EV (anti-Neg). Decreased levels of miR-210-3p in mPVEC and mPVEC-derived H-EV were validated by qPCR analysis (Figure S6). Then we injected mice in room air with H-EV (anti-miR-210), H-EV (anti-Neg), or PBS for 3 days and measured PH indices 3 weeks later (similar to the protocol for Figure 2a). We found that mice injected with H-EV (anti-Neg) had increased RVSP (Figure 5a), RV hypertrophy (Figure 5b), and pulmonary vessel remodeling (Figure 5c) similar to mice injected with H-EV (Figure 2), while mice injected with

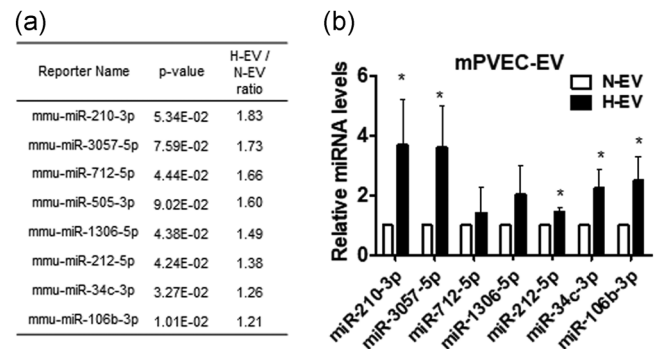


FIGURE 3 Hypoxia exposure alters miRNA cargo in endothelium-derived EV. EV released by mPVEC in room air (N) or hypoxia (H, 1% O₂, 24 h) were collected (N-EV or H-EV) and used for miRNA deep sequencing (a) followed by qRT-PCR validation (b). miRNA levels in H-EV were compared to that in N-EV. (a) miRNA deep sequencing result showed that hypoxia-induced expression of eight miRNAs in mPVEC-derived EV by more than 20%. (b) Five (miR-210-3p, 3057-5p, 212-5p, 34c-3p, and 106b-3p) out of eight identified miRNAs were confirmed to be induced in H-EV by qRT-PCR validation. Data are presented as mean \pm SEM. *, $p < 0.05$. EV, extracellular vesicles; H-EV, EV in hypoxia; miRNA, microRNA; mPVEC, mouse pulmonary vascular endothelial cells; qRT-PCR, quantitative real-time reverse transcription-polymerase chain reaction

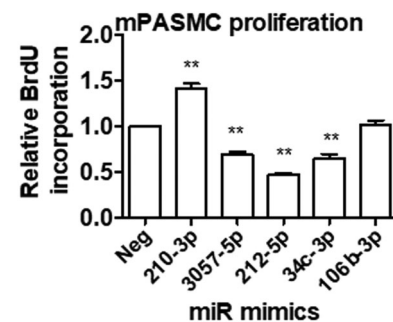


FIGURE 4 miRNAs in EV regulate PASM C proliferation. mPASM C were transfected with miRNA mimics for identified miRNAs in Figure 3. Forty-eight hours later, mPASM C proliferation was measured using BrdU proliferation assay. Relative mPASM C proliferation activity was analyzed by comparing the BrdU incorporation in each group to that in mPASM C transfected with negative control (Neg) mimics (set as 1). The result showed that miR-210-3p was the only identified miRNA that induces mPASM C proliferation, while miR-3057-5p, 212-5p, and 34c-3p suppressed mPASM C proliferation. Data are presented as mean \pm SEM. **, $p < 0.01$. BrdU, bromodeoxyuridine; EV, extracellular vesicles; miRNAs, microRNA; mPASM C, mouse PASM C; PASM C, pulmonary artery smooth muscle cells

H-EV (anti-miR-210), had no elevation in RVSP (Figure 5a), had significantly reduced RV hypertrophy (Figure 5b) and had attenuated pulmonary vessel wall remodeling (Figure 5c,d). These data indicate that

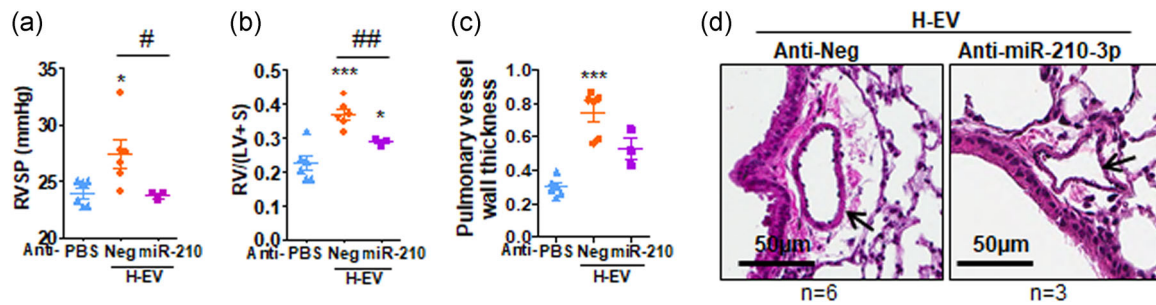


FIGURE 5 Inhibition of miR-210-3p in H-EV significantly attenuated H-EV-induced PH in mice in room air. mPVEC were transfected with miR-210-3p or negative control (Neg) inhibitors (anti-miR-210 or anti-Neg). Twenty-four-hour, mPVEC culture medium (containing transfection reagent) was refreshed with a medium free of FBS or vesicles and mPVEC were exposed to hypoxia (1% O₂). EV released from mPVEC were collected 24 or 48 h later (H-EV (anti-miR-210) or H-EV (anti-Neg)). Six- to eight-week-old C57BL/6 mice were injected with H-EV (anti-miR-210) or H-EV (anti-Neg) (10e8 EV per daily injection for three consecutive days, i.v., similar to Figure 2 (a) while they were in room air. Mice receiving PBS served as controls. Three weeks later, PH indices were measured. Our data show that inhibition of the miR-210-3p level in H-EV significantly attenuated H-EV-induced elevation of RVSP (a) and RV hypertrophy (b). Pulmonary vessel wall remodeling was also attenuated ($p = 0.047$) but power did not reach 0.8 (power = 0.77) (c,d). Arrows point to vessels. Data are presented as mean \pm SEM. * or *** versus PBS control, # or ## versus H-EV (anti-Neg). * or # $p < 0.05$; ##, $p < 0.01$; ***, $p < 0.001$. PBS: $n = 6$; H-EV (anti-Neg): $n = 6$; H-EV (anti-miR-210): $n = 3$. FBS, fetal bovine serum; H-EV, extracellular vesicles in hypoxia; i.v., intravenous; mPVEC, mouse pulmonary vascular endothelial cells; PH, pulmonary hypertension; RV, right ventricle; RVSP, right ventricular systolic pressure

miR-210-3p in H-EV plays a major role in H-EV-induced PH in mice in room air.

DISCUSSION

In this study, we demonstrated for the first time that PVEC-derived EV in hypoxia induce PASMCM proliferation in-vitro and induce PH in mice in room air (Figures 1 and 2). Though many extrinsic and intrinsic mechanisms for PASMCM proliferation exist and other constituents in EV cargo may be contributing to the increased PASMCM proliferation and PH in hypoxia, we have demonstrated an important contributory role of EV and their miRNA cargo in PH.

Recent studies have shown an association between dysregulated circulating levels of endothelium-derived EV and pathogenesis of PH.^{9,34} Tual-Chalot et al. demonstrated that EV obtained from the blood of rats exposed to hypoxia inhibited endothelium-dependent relaxation of rat pulmonary arteries.³⁵ Aliotta and colleagues found that healthy mice injected with EV (mostly exosomes) isolated from lung cells or plasma of MCT-treated mice developed significant RV hypertrophy and pulmonary vascular remodeling.³⁶ These studies are largely focused on EV from whole lungs or those in circulation, the cellular origin of which has not been determined. A recent study by Zhu et al. showed that cigarette smoke enhances EV generation from the endothelium, with spermine enrichment on their outer surface and cytosol, and that they contribute to SMC

constriction and proliferation, and consequently the development of PH.³⁷ However, from these studies our knowledge about the specific cargo in EV that was responsible for inducing vascular remodeling and PH is very limited.

We focused on the profile of miRNA cargo in the EV and the change in this profile induced by hypoxia. We found that miR-210-3p was increased in hypoxic EV (H-EV) and that H-EV could induce PASMCM proliferation. Although hypoxia can directly stimulate the expression of miR-210-3p in PASMCM and its role in hypoxia-induced PH has been previously reported by us and others,^{32,33} EV may also deliver an additional load of miR-210-3p to PASMCM in hypoxia and further contribute to hypoxia-induced PASMCM proliferation and pulmonary vessel remodeling. In this study, we demonstrated that inhibition of miR-210-3p in H-EV significantly attenuated the ability of H-EV to induce PH in mice in room air in-vivo (Figure 5), indicating that miR-210-3p in H-EV plays a major role in inducing pulmonary vascular remodeling and PH. Although we also identified anti-proliferative miRNAs, miR-3057-3p, 212-5p, 34c-3p, in their cargo (Figure 4), the net effect of H-EV is increased PASMCM proliferation in-vitro and PH in mice, which can be explained by the greater expression level of miR-210-3p in H-EV (Figure S5). The finding that EV cargo contains miRNAs that both stimulate as well as inhibit PASMCM proliferation suggests that under certain conditions the relative amounts of these miRNAs in EV may be modulated to either exacerbate or inhibit PASMCM proliferation and vascular remodeling. Certainly, it is

possible that other cargos (like proteins, etc.) in H-EV may also be transferred to induce PASMC proliferation and contributes to the development of PH. Further studies are warranted.

ACKNOWLEDGMENT

We thank UIC Electron Microscopy Core, Fluorescence Imaging Core, Research Informatics Core and Research Histology and Tissue Imaging Core (RHTIC) for their professional services. This study is partly supported by an NIH R01HL123804 (Raj and Zhou), an American Lung Association Biomedical Research Award RG-416135 (Chen), an American Heart Association Career Development Award 18CDA34110301 (Chen), and a Gilead Sciences Research Scholars Program in Pulmonary Arterial Hypertension (Chen), an NIH 1R56-HL141206-01 (Raj and Chen), a Chicago Biomedical Consortium Catalyst Award (Raj, Chen, and Hubbell).

CONFLICT OF INTERESTS

The authors declare that there are no conflict of interests.

ETHICS STATEMENT

All animals were cared for in accordance with the University of Illinois at Chicago Animal Care Policy. Animal experimental protocols were reviewed and approved by the Institutional Animal Care and Use Committee.

AUTHOR CONTRIBUTIONS

Tianji Chen and J. Usha Raj contributed to the conception and design of the work and interpretation of data; Tianji Chen, Miranda R. Sun, Qiyuan Zhou, Alyssa M. Guzman, Ramaswamy Ramchandran, Jiwang Chen, and Balaji Ganesh contributed to the acquisition of data; Tianji Chen, Miranda R. Sun, Ramaswamy Ramchandran, and Balaji Ganesh contributed to the analysis of data. Tianji Chen and J. Usha Raj have drafted the work and Miranda R. Sun also contributed to editing the manuscript.

REFERENCES

- Gao Y, Chen T, Raj JU. Endothelial and smooth muscle cell interactions in the pathobiology of pulmonary hypertension. *Am J Respir Cell Mol Biol*. 2016;54:451–60.
- Morrell NW, Adnot S, Archer SL, Dupuis J, Lloyd Jones P, MacLean MR, McMurtry IF, Stenmark KR, Thistlethwaite PA, Weissmann N, Yuan JX, Weir EK. Cellular and molecular basis of pulmonary arterial hypertension. *J Am Coll Cardiol*. 2009;54:S20–31.
- Giaid A, Saleh D. Reduced expression of endothelial nitric oxide synthase in the lungs of patients with pulmonary hypertension. *N Engl J Med*. 1995;333:214–21.
- Moncada S, Higgs A. The L-arginine-nitric oxide pathway. *N Engl J Med*. 1993;329:2002–12.
- Fukuroda T, Kobayashi M, Ozaki S, Yano M, Miyachi T, Onizuka M, Sugishita Y, Goto K, Nishikibe M. Endothelin receptor subtypes in human versus rabbit pulmonary arteries. *J Appl Physiol* (1985). 1994;76:1976–82.
- McCulloch KM, MacLean MR. EndothelinB receptor-mediated contraction of human and rat pulmonary resistance arteries and the effect of pulmonary hypertension on endothelin responses in the rat. *J Cardiovasc Pharmacol*. 1995; 26(Suppl 3):S169–76.
- Davie N, Haleen SJ, Upton PD, Polak JM, Yacoub MH, Morrell NW, Wharton J. ET(A) and ET(B) receptors modulate the proliferation of human pulmonary artery smooth muscle cells. *Am J Respir Crit Care Med*. 2002;165:398–405.
- Kizub IV, Strielkov IV, Shaifita Y, Becker S, Prieto-Lloret J, Snetkov VA, Soloviev AI, Aaronson PI, Ward JP. Gap junctions support the sustained phase of hypoxic pulmonary vasoconstriction by facilitating calcium sensitization. *Cardiovasc Res*. 2013;99:404–11.
- Loyer X, Vion AC, Tedgui A, Boulanger CM. Microvesicles as cell-cell messengers in cardiovascular diseases. *Circ Res*. 2014; 114:345–53.
- Abels ER, Breakefield XO. Introduction to extracellular vesicles: biogenesis, RNA cargo selection, content, release, and uptake. *Cell Mol Neurobiol*. 2016;36:301–12.
- Thery C, Ostrowski M, Segura E. Membrane vesicles as conveyors of immune responses. *Nat Rev Immunol*. 2009;9: 581–93.
- György B, Szabó TG, Pásztói M, Pál Z, Misják P, Aradi B, László V, Pállinger E, Pap E, Kittel A, Nagy G, Falus A, Buzás EI. Membrane vesicles, current state-of-the-art: emerging role of extracellular vesicles. *Cell Mol Life Sci*. 2011;68: 2667–88.
- Baietti MF, Zhang Z, Mortier E, Melchior A, Degeest G, Geeraerts A, Ivarsson Y, Depoortere F, Coomans C, Vermeiren E, Zimmermann P, David G. Syndecan-syntenin-ALIX regulates the biogenesis of exosomes. *Nat Cell Biol*. 2012;14:677–85.
- Colombo M, Moita C, van Niel G, Kowal J, Vigneron J, Benaroch P, Manel N, Moita LF, Théry C, Raposo G. Analysis of ESCRT functions in exosome biogenesis, composition and secretion highlights the heterogeneity of extracellular vesicles. *J Cell Sci*. 2013;126:5553–65.
- Prokopi M, Pula G, Mayr U, Devue C, Gallagher J, Xiao Q, Boulanger CM, Westwood N, Urbich C, Willeit J, Steiner M, Breuss J, Xu Q, Kiechl S, Mayr M. Proteomic analysis reveals presence of platelet microparticles in endothelial progenitor cell cultures. *Blood*. 2009;114:723–32.
- György B, Módos K, Pállinger E, Pálóczi K, Pásztói M, Misják P, Deli MA, Sipos A, Szalai A, Voszka I, Polgár A, Tóth K, Csete M, Nagy G, Gay S, Falus A, Kittel A, Buzás EI. Detection and isolation of cell-derived microparticles are compromised by protein complexes resulting from shared biophysical parameters. *Blood*. 2011;117:e39–48.
- Hergenreider E, Heydt S, Tréguer K, Boettger T, Horrevoets AJ, Zeiher AM, Scheffer MP, Frangakis AS, Yin X, Mayr M, Braun T, Urbich C, Boon RA, Dimmeler S. Atheroprotective communication between endothelial cells and smooth muscle cells through miRNAs. *Nat Cell Biol*. 2012;14: 249–56.

18. Sódar BW, Kittel Á, Pálóczi K, Vukman KV, Osteikoetxea X, Szabó-Taylor K, Németh A, Sperlág B, Baranyai T, Giricz Z, Wiener Z, Turiák L, Drahos L, Pállinger É, Vékey K, Ferdinandy P, Falus A, Buzás EI. Low-density lipoprotein mimics blood plasma-derived exosomes and microvesicles during isolation and detection. *Sci Rep.* 2016; 6:24316.
19. Raposo G, Stoorvogel W. Extracellular vesicles: exosomes, microvesicles, and friends. *J Cell Biol.* 2013;200:373–83.
20. Gurunathan S, Kang MH, Jeyaraj M, Qasim M, Kim JH. Review of the isolation, characterization, biological function, and multifarious therapeutic approaches of exosomes. *Cells.* 2019; 8:307.
21. Maas SLN, Breakefield XO, Weaver AM. Extracellular vesicles: unique intercellular delivery vehicles. *Trends Cell Biol.* 2017;27:172–88.
22. Niwa R, Slack FJ. The evolution of animal microRNA function. *Curr Opin Genet Dev.* 2007;17:145–50.
23. Williams AE. Functional aspects of animal microRNAs. *Cellular and molecular life sciences: CMLS.* 2008;65:545–62.
24. Davis-Dusenbery BN, Hata A. MicroRNA in cancer: the involvement of aberrant microRNA biogenesis regulatory pathways. *Genes Cancer.* 2010;1:1100–14.
25. Davis-Dusenbery BN, Wu C, Hata A. Micromanaging vascular smooth muscle cell differentiation and phenotypic modulation. *Arterioscler Thromb Vasc Biol.* 2011;31:2370–7.
26. Chen T, Zhou G, Zhou Q, Tang H, Ibe JC, Cheng H, Gou D, Chen J, Yuan JX, Raj JU. Loss of microRNA-17 approximately 92 in smooth muscle cells attenuates experimental pulmonary hypertension via induction of PDZ and LIM domain 5. *Am J Respir Crit Care Med.* 2015;191:678–92.
27. György B, Szabó TG, Turiák L, Wright M, Herczeg P, Lédeczi Z, Kittel A, Polgár A, Tóth K, Dérfalvi B, Zelenák G, Böröcz I, Carr B, Nagy G, Vékey K, Gay S, Falus A, Buzás EI. Improved flow cytometric assessment reveals distinct microvesicle (cell-derived microparticle) signatures in joint diseases. *PLOS One.* 2012;7:e49726.
28. del Conde I, Shrimpton CN, Thiagarajan P, López JA. Tissue-factor-bearing microvesicles arise from lipid rafts and fuse with activated platelets to initiate coagulation. *Blood.* 2005; 106:1604–1611.
29. Nguyen DB, Ly TB, Wesseling MC, Hittinger M, Torge A, Devitt A, Perrie Y, Bernhardt I. Characterization of microvesicles released from human red blood cells. *Cell Physiol Biochem.* 2016;38:1085–99.
30. Faught E, Henrickson L, Vijayan MM. Plasma exosomes are enriched in Hsp70 and modulated by stress and cortisol in rainbow trout. *J Endocrinol.* 2017;232:237–46.
31. Mathew B, Ravindran S, Liu X, Torres L, Chennakesavalu M, Huang CC, Feng L, Zelka R, Lopez J, Sharma M, Roth S. Mesenchymal stem cell-derived extracellular vesicles and retinal ischemia-reperfusion. *Biomaterials.* 2019;197:146–60.
32. Gou D, Ramchandran R, Peng X, Yao L, Kang K, Sarkar J, Wang Z, Zhou G, Raj JU. miR-210 has an antiapoptotic effect in pulmonary artery smooth muscle cells during hypoxia. *Am J Physiol Lung Cell Mol Physiol.* 2012;303:L682–91.
33. White K, Lu Y, Annis S, Hale AE, Chau BN, Dahlman JE, Hemann C, Opotowsky AR, Vargas SO, Rosas I, Perrella MA, Osorio JC, Haley KJ, Graham BB, Kumar R, Saggari R, Saggari R, Wallace WD, Ross DJ, Khan OF, Bader A, Gochuico BR, Matar M, Polach K, Johannessen NM, Prosser HM, Anderson DG, Langer R, Zweier JL, Bindoff LA, Systrom D, Waxman AB, Jin RC, Chan SY. Genetic and hypoxic alterations of the microRNA-210-ISCU1/2 axis promote iron-sulfur deficiency and pulmonary hypertension. *EMBO Mol Med.* 2015;7:695–713.
34. Amabile N, Heiss C, Real WM, Minasi P, McGlothlin D, Rame EJ, Grossman W, De Marco T, Yeghiazarians Y. Circulating endothelial microparticle levels predict hemodynamic severity of pulmonary hypertension. *Am J Respir Crit Care Med.* 2008;177:1268–75.
35. Tual-Chalot S, Guibert C, Muller B, Savineau JP, Andriantsitohaina R, Martinez MC. Circulating microparticles from pulmonary hypertensive rats induce endothelial dysfunction. *Am J Respir Crit Care Med.* 2010;182:261–8.
36. Aliotta JM, Pereira M, Amaral A, Sorokina A, Igbinoza Z, Hasslinger A, El-Bizri R, Rounds SI, Quesenberry PJ, Klinger JR. Induction of pulmonary hypertensive changes by extracellular vesicles from monocrotaline-treated mice. *Cardiovasc Res.* 2013;100:354–62.
37. Zhu L, Xiao R, Zhang X, Lang Y, Liu F, Yu Z, Zhang J, Su Y, Lu Y, Wang T, Luo S, Wang J, Liu ML, Dupuis J, Jing ZC, Li T, Xiong W, Hu Q. Spermene on endothelial extracellular vesicles mediates smoking-induced pulmonary hypertension partially through calcium-sensing receptor. *Arterioscler Thromb Vasc Biol.* 2019;39:482–95.

SUPPORTING INFORMATION

Additional supporting information may be found in the online version of the article at the publisher's website.

How to cite this article: Chen T, Sun MR, Zhou Q, Guzman AM, Ramchandran R, Chen J, Ganesh B, Raj JU. Extracellular vesicles derived from endothelial cells in hypoxia contribute to pulmonary artery smooth muscle cell proliferation in-vitro and pulmonary hypertension in mice. *Pulm Circ.* 2022;12:e12014.
<https://doi.org/10.1002/pul2.12014>